Limitations and Capabilities of the Slanted Spectrogram Analysis Tool for SAR-Based Detection of Multiple Vibrating Targets

Adebello Jelili, Balu Santhanam, and Majeed Hayat
Department of Electrical and Computer Engineering, University of New Mexico,
Albuquerque, NM 87131 USA

***Abstract*—The recently developed improved spectrograms that use the discrete fractional fourier transform (DFrFT) are used to evaluate multiple vibration signatures that represent targets in synthetic aperture radar (SAR) data. Multiple ground target vibrations that introduce phase modulation in the SAR returned signals are examined using standard pre-processing of the return waveform signal followed by the application of the DFrFT. In this paper, we study the capabilities of these spectrogram tools with the intent of extending their limits by varying the characteristic features associated with each vibrating target which result in different outputs. The performance of the fractional spectrogram tools, under the effects of various parameters is used to clarify the limitations and advantages of these modified fractional spectrograms for SAR-based vibrometry applications.**

***Index Terms*— synthetic aperture radar, discrete fractional Fourier transform, micro-Doppler effect, vibration estimation, clutter.**

I. Introduction

Radar has long been used for military and non-military purposes in a wide variety of applications such as imaging, guidance, remote sensing and global positioning. Vibration signatures associated with objects such as active structures and vehicles can bear vital information about the type and integrity of these objects [3]. These vibrating objects cause phase modulation of the azimuth phase history for a SAR system and this phase modulation is seen as a time-dependent micro-Doppler frequency [8] which is useful for analyzing such signals with appropriate time-frequency methods in order to preserve it superior resolution potential [2].

Implementation of the DFrFT, which is a generalization of the Discrete Fourier Transforms (DFT), shows promise for multicomponent chirp parameter estimation as it generates a strong peak for each chirp whose location in the 2D transform plane corresponds to the specific center frequency and chirp rate [6].

In this paper, we will describe the application of previously developed improved DFrFT-based spectrograms [6] on SAR data in terms of three criteria in order to properly evaluate and clarify the limitations and usefulness of these tools. Specifically, we explore the connection between vibration frequencies and amplitudes on the number of side-lobes present in the spectrograms. We further examine the effects of the chirp rates and clutter on the ability of these spectrograms in detecting vibrating targets.

This work was supported by the United States Department of Energy (Award No. DE-NA0002494) and the National Nuclear Security Administration (NA-221)

II. Synthetic Aperture Radar

A. Motion Model

Fig 1, depicts a three-dimensional SAR flight geometry, with a vibrating target located at the origin. The nominal line-of-sight distance from the target to the radar sensor is r_o, with the radar sensor located at polar angles ψ and φ to the target. Let $r_d(t)$ denote the projection of the vibration displacement onto the line-of-sight from the target to the SAR sensor, the range of the vibrating target becomes

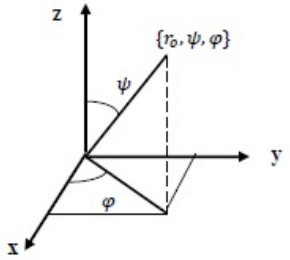

Fig. 1: Three dimensional SAR flight co-ordinate system for the description of an oscillating point target. The vibrating target is located at (r_o, Ψ, φ)

$$r(t) \approx r_o - r_d(t). \quad (1)$$

In this paper, we consider the case of broadside spotlight-mode SAR for which the aforementioned approximation is valid [2].

B. Signal Model

The small range perturbation of the vibrating target modulates the collected SAR phase history [7]. Consider a spotlight-mode SAR whose sent pulse is a chirp signal, with carrier frequency and the chirp rate f_c and K, respectively. Each returned SAR pulse is demodulated by the sent pulse delayed appropriately by the round-trip time to the center of the illuminated patch. A demodulated pulse can be written as [2]

$$r(t) = \sum_i \sigma_i \exp\left[-j\frac{4\pi(r_i - r_c)}{c}(f_c + K(t - \frac{2r_c}{c})\right], \quad (2)$$

where σ_i is the reflectivity of the ith scatterer, c is the propagation speed of the pulse, and r_c is the distance from

the patch center to the antenna [3], [4]. Range compression is applied to the phase history to separate the scatterers in range. Fig 2 shows the magnitude of the range-compressed SAR phase history containing the vibrating point target. Assuming that all scatterers at a specific range are static, the range-compressed phase history at this specific range can be written as

$$x[n] = \sum_i \sigma_i[n] \exp[-j(f_y y_i n - \frac{4\pi f_c}{c} r_i + \varphi_i)] + w[n], \quad (3)$$

for $0 \leq n < N_I$, where y_i is the cross-range position, φ_i represent additional phase terms, and $w[n]$ is additive noise with f_y as the known imaging factor according to [7].

We define the *signal of interest* (SoI) as the range line in the range-compressed phase history containing vibrating targets. In this paper, we consider cases for which the vibrating scatterer is well-separated from other scatterers in range (e.g., this may be possible by choosing a proper data collection orientation). In this case, the SoI can be written as

$$x_i[n] = \sigma_i[n] \exp[-j(f_y \bar{y} n - \frac{4\pi f_c}{c} r_d[n] + \varphi)] + w[n]. \quad (4)$$

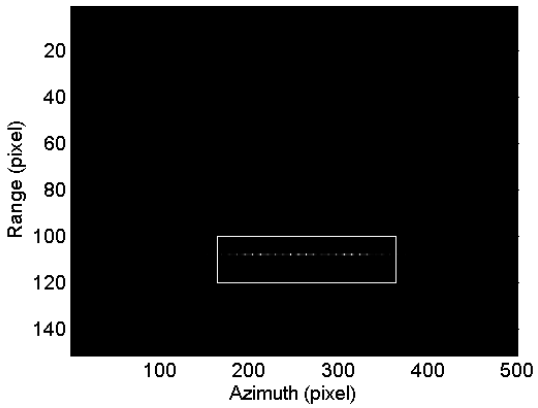

Fig. 2: The reconstructed SAR Image for vibrating target that introduces ghost lines along the azimuth direction.

III. Improved Spectrograms

The generalizations of the DFT such as the DFrFT and in particular, the centered version of the DFrFT based on the Grunbaum tridiagonal commutor [3] have been shown to possess the capability to concentrate a chirp signal in a few transform coefficients [4]. The improved spectrogram assumes a multicomponent sinusoidal model over the analysis frame by using the CDFrFT and the MA-CDFrFT to decompose the signal frame into the superposition of harmonically related chirp signals. In this paper, we apply the slanted spectrogram framework to non-harmonic chirp components using both piece-wise linear and polynomial fitted methods according to [10]. Simulation results on synthetic chirps indicate that these generalized slanted spectrograms provide sharper features when the chirp components are not harmonically

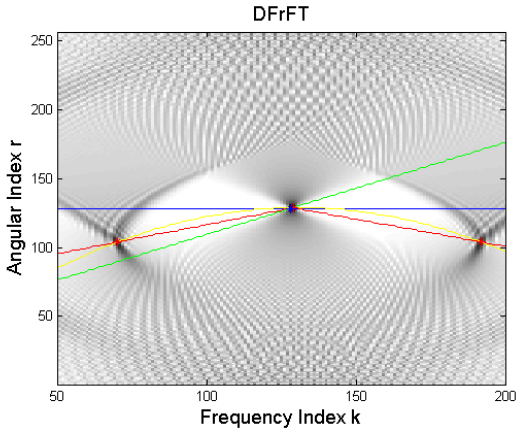

Fig. 3: DFrFT magnitude of a frame of the SAR signal, The piece-wise linear spectrogram (red) passes through all the peaks, the polynomial spectrogram (yellow) also passes all peaks, the slanted spectrogram (green) accommodates only one peak and ignores the other two, the conventional spectrogram (blue) also ignores two peaks.

related. So the DFrFT analysis tool shows promise for the analysis of signals frequency chirping (i.e. linearly changing) [6] such as radar as employed in this paper. The conventional spectrogram assumes a multicomponent sinusoidal model over the analysis frame while the slanted spectrogram replaces that sinusoidal assumption with a multicomponent harmonically related chirp model. However, the data used in this paper contains non-harmonically related chirps, therefore two DFrFT based spectrograms; polynomial fitted and piece-wise linear approaches were employed, which provide sharper features than the slanted and conventional spectrogram as described in [7].

IV. Simulation and Performance Analysis

We use a SAR signal containing three vibrating objects with varying amplitudes and vibrating frequencies respectively for system parameters described for both noise free case and noise case. Using an initial sampling frequency of 3.216 MHz, a down-sampler is applied on the data to a sampling rate of 40 KHz. We calculated the spectrograms of the SAR signal using 256 point DFrFT for all cases and a 256 point Hamming window with 255 samples of overlap. The polynomial orders were varied throughout the experiment and the radar signals contained complex signals with three chirp components.

The characteristics of this tool and its application to SAR are dependent on different parameters which include (a) the vibrating frequencies, (b) the amplitude of targets, (c) the chirp-rate effects, and (d) clutter and noise. During this investigation and evaluation, the polynomial fitted and the piece-wise linear produce the same results for most part, considering that SAR signals are non-harmonically related. The line connecting the zero chirp-rate and zero frequency coordinates to the largest peaks does not pass through all the spectral peaks, therefore the conventional spectrogram and the slanted spectrogram produced blurry results since both spectrogram benefits only

one peak and ignore two peaks according to Fig 3. The polynomial fitted and the piece-wise linear spectrum provide sharper features and clearer spectrograms since they both take into accounts all the peaks. We used SAR signals with different combinations of vibrating frequencies according to Table I. for different cases.

A. *Effects of vibration frequencies and amplitudes*

The frequency and amplitude of the SAR return signal measure the vibration signatures of both the target and clutter in the return waveform. Therefore, considering three vibrating targets by varying and increasing their respective amplitudes and vibrating frequencies increases the number of side lobes present in the spectrograms as shown in Fig 4-6. Following these results, the degree of vibration present in the input data can be estimated and evaluated at different values. From the conducted simulations, it can be deduced that the presence of side-lobes is proportional to the degree of non-stationarity received from the SAR return signals and changes in the center frequencies have no effect on the output results. Comparing the different spectrogram outputs, the conventional performs equally well as the slanted spectrogram because the latter ignores most peaks while both of the improved DFrFT spectrograms locate all peaks present.

Table I: Different combinations of targets parameter values used for evaluating the improved spectrograms, slanted spectrogram and convention spectrogram.

	Case I			*Case II*			*Case III*		
Target	*A*	*B*	*C*	*A*	*B*	*C*	*A*	*B*	*C*
Amplitude(mm)	1	1	1	1	10	20	10	20	1
Frequency(Hz)	2	4	2	2	2	2	1	2	4

Case I : The old-slanted spectrogram ignores two of the peaks. This results from the fact that different frequencies generate a non-harmonically related signal where the old-slanted spectrogram cannot locate all three peaks as shown in Fig 4.

Case II : Presence of larger side-lobes occurs with each of the spectrogram tool, the conventional and old-slanted ignore most of the peaks and produce larger side-lobes than the improved spectrogram as shown in Fig 5. Though, the polynomial spectrogram output does not match that of the piece-wise spectrogram, the peaks for each target can still be seen clearly. These results can be deduced from the facts that the presence of targets with large vibration amplitude produce blurry peaks for the slanted spectrogram and generate larger side lobes for the improved spectrograms.

Case III : This comprises of the combination of CASE II and III with greater differences in the values of the frequencies and amplitudes respectively. These changes in vibration frequencies and amplitudes result in the presence of side-lobes for spectrograms (I), (III) and (IV) since the amplitudes have values of 10 mm, 20 mm and 1 mm.

Estimating the frequency and amplitude thresholds due to the results from the above cases, we can derive boundaries for the vibration frequency that can be detected using the spectrogram tools. We know from [7] that the vibration frequency f_m is linearly proportional to the nominal velocity of the moving or rotating target. Correlating this to the level of non-stationarity of the return signal, we can deduce that f_m is proportional to the level of vibration via stationarity deviations: $S_{df} = 1 - f_{st}/f_m$ and $S_{da} = 1 - A_{st}/A_m$, where f_m is the vibration frequency, f_{st} is the static object frequency, and A_{vb} ,A_{st} are the amplitudes of the vibrating and static targets.

The stationarity deviation percentage S_d was calculated and the threshold for detection was found within $S_{df} \in [0, 0.85]$ for the improved spectrograms and $S_d = 0.667$ for both conventional and slanted spectrogram. Using the same relationship for the amplitude, the tools fails to detect all targets out of range of $S_{da} \in [0, 0.98]$. Therefore, we can exploit this information to determine the level of non-stationarity a signal contains from the width of side-lobes in the output graphs, which in turn gives us the approximate value of f_m, A_{vb} and velocity of the moving target.

B. *Chirp-rate effect*

SAR signals can in general be comprised of non-harmonically related chirp components resulting in the peaks not connected by a single line and not passing through the zero chirp-rate and zero frequency coordinates as shown in Fig 3. In order to evaluate the effect of these chirp-rates on the improved spectrograms, we look at SAR chirp signals comprised of three non-harmonic components with chirp rates $Cr = [0.01, 0.05, 0.1]\, rad/samples^2$ having vibrating frequencies of 1 Hz, 2 Hz and 2 Hz for each target respectively. The polynomial fitted and the piece-wise linear methods take into account all the peaks regardless of the value of Cr as shown in Fig 7-8.

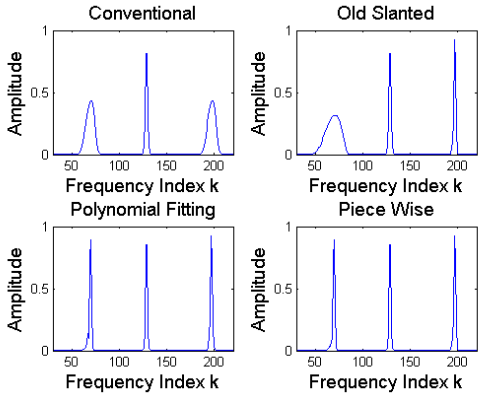

Fig. 7: Extracted spectrograms for a frame of non-harmonically related SAR chirp signal using $Cr = 0.05\, rad/samples^2$.

Estimating the chirp-rate thresholds from the simulation results, we observed that the higher the value of the chirp

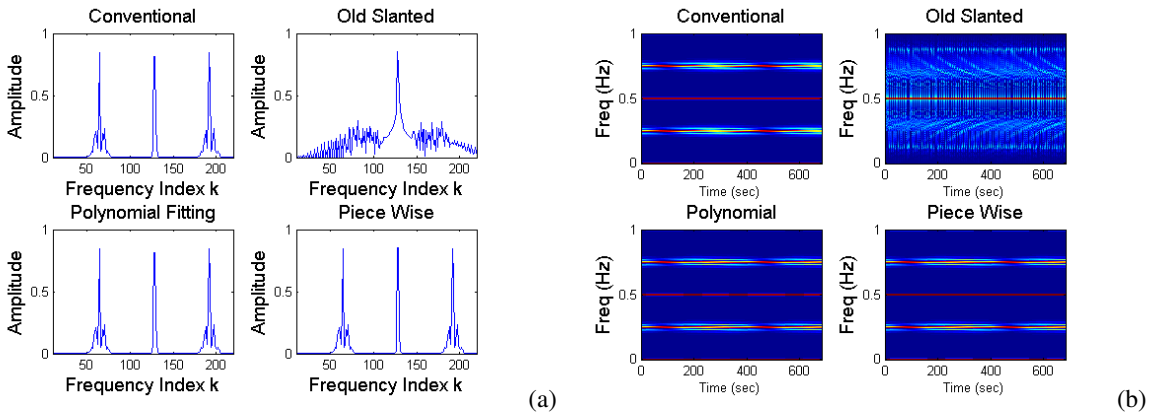

Fig. 4: (a) Extracted spectrograms for a frame of a non-harmonically related SAR chirp signal. (b) Spectrogram of a SAR signal containing three vibrating target signal using spectrogram tools (I), (II), (III) and (IV) for **CASE I**.

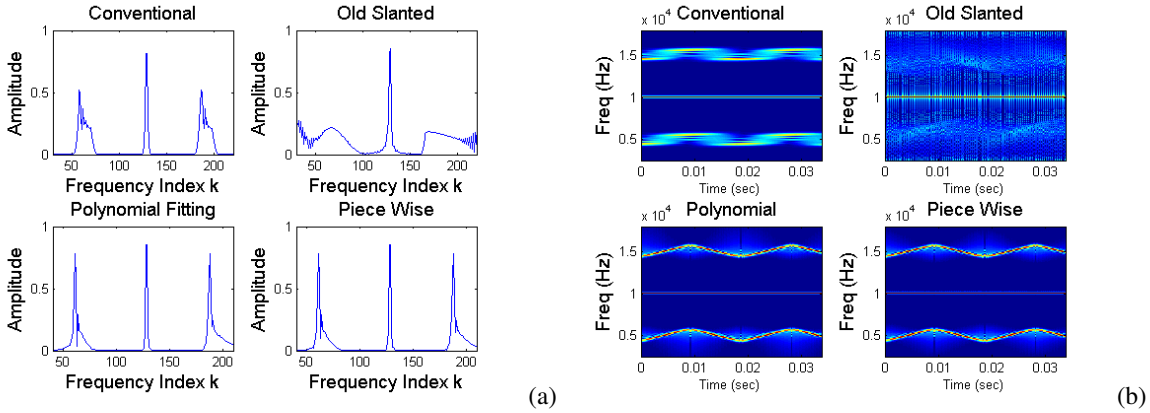

Fig. 5: (a) Extracted spectrograms for a frame of a non-harmonically related SAR chirp signal. (b) Spectrogram of a SAR signal containing three vibrating target signal using spectrogram tools (I), (II), (III) and (IV) for **CASE II**.

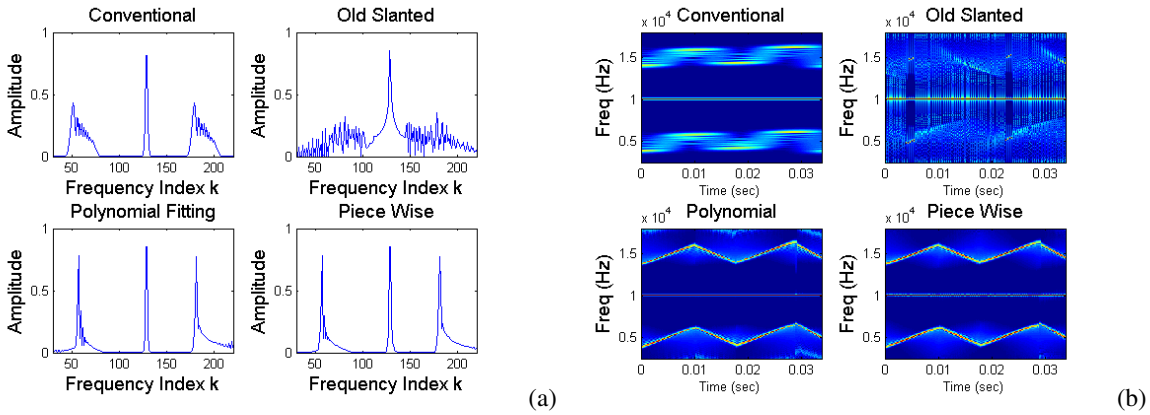

Fig. 6: (a) Extracted spectrograms for a frame of a non-harmonically related SAR chirp signal. (b) Spectrogram of a SAR signal containing three vibrating target signal using spectrogram tools (I), (II), (III) and (IV) for **CASE III**.

rates K, the higher the degree of non-stationarity of the output signals. Fig 7-8 shows that as the value of K increases the slanted and conventional spectrogram gradually fail to detect all targets. Therefore, we can conclude that if the minimum measurable chirp rate for the slanted spectrogram ($K_{min} = 0.001 rad/samples^2$) denotes the stationary target's chirp rate

and using K_{min} as a lower limit measure for detecting the vibration acceleration, since it had been established in [8] that the chirp rate K is directly proportional to the vibration acceleration a_v for a target signal. For values of $K > K_{min}$, the ratio of detection $\rho_k = K/K_{min}$ was used to estimate the threshold for the slanted spectrogram to be within range $1 < \rho_k \leq 4.5$ and the improved spectrogram detects all target regardless of the value of K. This can be used to estimate the value of the vibration acceleration a_v of targets.

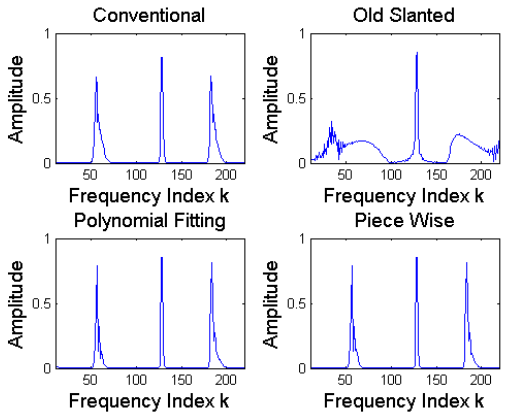

Fig. 8: Extracted spectrograms for a frame of non-harmonically related SAR chirp signal using $Cr = 0.1\,rad/samples^2$.

C. Clutter Effects

Using vibrating frequencies of 1 Hz each and amplitude of $(1, 1, 10)$ mm respectively with clutter corresponding to a gamma-theta value of 1 which is fixed with pixel size of $N \times M$ to derive the SCR scalar as a normalizing factor, along SCR and SNR of $20dB$ each. As is evident from Fig 9, all targets were detected by the improved spectrograms even with low values of SNR and SCR, but the slanted and conventional exhibit some target suppression due to high interference of the clutter and noise even after appropriate filtering.

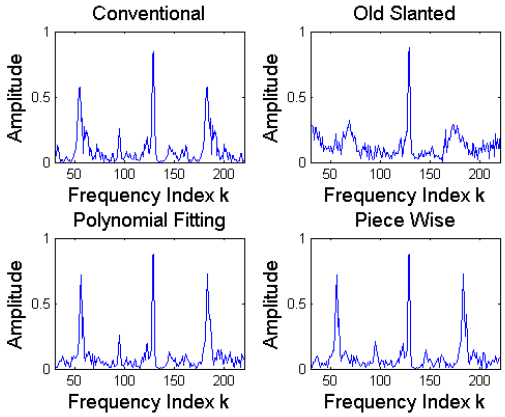

Fig. 9: Extracted spectrograms for the corrupted SAR signal with three targets having the same vibration frequencies of 1 Hz each.

V. Conclusion

In this paper, we carried out a qualitative evaluation of the limits and capabilities of the slanted spectrogram in comparison with the improved spectrograms by evaluating the performance of each tool using parameter variations. From the results, we can conclude that varying the characteristics of the input signal, the performance of the improved spectrograms outperforms the old-slanted spectrogram in terms of its ability to clearly detect the number of targets present in the SAR signals without distortions or elimination of targets. We also noticed that a minimum chirp rate or vibration frequency/amplitude is needed before each of these improved fractional spectrogram tools can provide improvement over the slanted spectrogram.

Therefore, from the analysis of each tool it can be concluded that the non-stationary character of the return signal manifests as side-lobes in the spectrograms which can be observed when an increase in the chirp rate or vibration frequency and amplitude of the returned signal occurs. In general, we can infer that the non-stationarity of the signal is dependent on the values of A_{vb}, K and f_m, which can be used for the characterization of target variables for recognition purposes. This vital information will be used in future work to establish a detailed relationship between these parameters and to populate a database of different target environments.

References

[1] I. G. Cumming and F. H. Wong, "Digital processing of synthetic aperture radar data: algorithm and implementation," Artech House, Norwood, MA, 2005.

[2] C. V. Jakowatz, and D. E. Wahl, and P. H. Eichel, and D. C. Ghiglia and P. A. Thompson, "Spotlight-Mode synthetic aperture radar: A signal processing approach," Springer-Verlag, New York, 1996.

[3] V. C. Chen, and F. Li, and S. S. Ho, and H. Wechsler, "Micro-Doppler effect in radar: Phenomenon, model, and simulation study," *IEEE Trans. Aerosp. Electron. Syst.*, Vol. 42, No. 1, pp. 2-21, January, 2006.

[4] Q. Wang, and M. Xing, and G. Lu, and Z. Bao, "High-resolution three-dimension radar imaging for rapidly spinning target," *IEEE Trans. Geosci. Remote Sens.*,Vol. 46, No. 1, pp. 22-30, January, 2008.

[5] L. S. Reddy, and B. Santhanam, and M. M. Hayat, "Multicomponent chirp demodulation using discrete fractional Fourier transform," *IEEE Proc. 12th Digital Signal Processing Workshop*, pp. 418-422, Sept., 2006.

[6] J. G. Vargas-Rubio and B. Santhanam, "An Improved Spectrogram Using The Multi-angle Centered Discrete Fractional Fourier Transform," *Proc. of ICASSP*, pp. 505-508, 2005.

[7] Q. Wang, and B. Santhanam, and M. M. Hayat, and R. Dunkel, and T. Atwood, and A. W. Doerry and M. Pepin, and R. J Beach, and W. Gerstle, "SAR-based vibration estimation using the discrete fractional fourier transform," *IEEE Trans. Geosci. Remote Sens.*, Vol. 50, No. 10, pp. 4145-4156, Oct., 2012.

[8] Q. Wang, and B. Santhanam, and M. M. Hayat, and R. Dunkel, and T. Atwood et. al., "Demonstration of target vibration estimation in synthetic aperture radar imagery," *Proc. of IEEE Int. Geosci. Remote Sens. Symp.*, pp. 4083-4086, 2011.

[9] Shen Chiu, "Clutter effects on ground moving target velocity estimation with SAR Along-Track Interferometry," *Proc. IEEE Int. Geosci. Remote Sens. Symp.*, Vol. 2, pp. 1314-1319, July, 2003.

[10] O. Agcaoglu, and B. Santhanam, and M. Hayat, "Improved Spectrograms using Discrete Fraction Fourier Transform," *Proc. of IEEE DSP/SPED Workshop*, pp. 80-85, Aug., 2013.